A Waveform Model for Bistatic Radar With Arbitrary Long Coherent Processing Interval

1st Tomas McKelvey
Electrical Engineering
Chalmers University of Technology
Gothenburg, Sweden
tomas.mckelvey@chalmers.se

2nd Patrik Dammert
Future Technologies Radar and Systems
Surveillance, Saab AB
Gothenburg, Sweden
patrik.dammert@saabgroup.com

***Abstract*—A model for bistatic radar waveforms with an arbitrary long coherent processing interval (CPI) is presented. The model describes the received waveform in the time domain accounting for the varying propagation delay due to the bistatic range variation during the CPI. The model represents the received waveform, accounting for relative constant velocity motion between radar platforms and target. Traditional methods often simplify this effect, leading to performance losses that can become severe for long CPI. The proposed model supports arbitrary transmitted waveforms including continuous wave (CW) operation, long CPIs, and varying positions and velocities of the transmitter, receiver, and target. It also extends to multichannel receivers. The developed model can readily be used in simulations to quantify the performance loss when evaluating suboptimal detectors based on simplifying model assumption. Simulations demonstrate the use of the model to highlight the impact of target velocity and CPI length on the performance when using the classical approximate Kronecker structure (space, fast-time, slow-time) processing model. The introduced model pave the way for future research on developing fast and accurate processing schemes for different multichannel radar systems utilising long CPI.**

***Index Terms*—bistatic radar, radar detection, coherent detection, array signal processing**

I. Introduction

In coherent radar processing, the received waveform shape is fully utilized to maximize the signal to noise ratio (SNR) in a detector [1]. The processing time interval is then called a coherent processing interval (CPI). To achieve full coherence during the CPI, the processing needs an accurate model of the received pulse shape. For a scenario when there is a relative velocity between the radar platform and the target, the received waveform is stretched or compressed in time, an effect that can be described with a non-linear propagation delay function. However, if the CPI is short enough, the waveform is repetitive or with a sufficiently small pulse bandwidth, the processing can be split into handle range and relative velocity separately. Classical pulse Doppler radar processing is based on this simplification. The stretch and compression effect has been studied and analysed in many radar signal processing publications. One of the absolute first references is the seminal analysis in reference [2]. The reference describes the constraint that the target range walk and Doppler walk (related to stretch and compression effect) needs to be smaller than the corresponding resolutions in range and Doppler. The range constraint may be written as that the time-bandwidth product needs to be smaller than the wave propagation speed divided by twice the target radial velocity. The Doppler constraint may be written as that the integration time needs to be smaller than the radar wavelength divided by twice the target Doppler variation. Since this reference, there is a multitude of analyses and processing methods for different monostatic radar settings. For example, processing for moving targets with substantial range and Doppler walk in very long CPIs has attracted much attention, see e.g. references [3]–[10]. Of special interest is the introduction of the Keystone processing method in reference [9] which mitigates large linear range walk (targets with radial velocities). There is a vast body of publications on variations of the Keystone processing method. Targets that also have a tangential velocity will experience a Doppler walk, and there are a few methods that mitigate such effects, see e.g. [11]–[16] For a passive, or a noise, radar, the problem has also attracted interest. See e.g. description in references [17], [18]. and a few cases where Keystone processing have also been used [19]–[22]. The bulk of methods referred to above all introduce a 'fast-time' and 'slow-time' re-structuring of the received data. In a multichannel receiver, a target's angular walk also needs to be considered and utilized. For a sufficiently short CPI or small target velocities, the target direction vector can be assumed constant and processing in angle domain can be performed independent of range and velocity processing. However, as the classical range, angle and velocity processing is based on a simplified waveform model it will yield a loss in performance as compared to the optimal performance. The effect becomes more pronounced, and potentially severe, when above target walk criteria is not met for the CPI.

To enable an objective quantification of how various simplifying assumptions impact the overall performance of a given method, a model, free from these assumptions is needed. In this contribution, we introduce a bistatic model for the shape of the received multichannel waveform that is valid for an arbitrary transmitted waveform, an arbitrarily long coherent processing interval (CPI), and arbitrary positions and velocities of the transmitter platform, receiver platform, and target. We assume that the velocity vectors remain constant during the CPI. The model further assumes that the complex-valued radar cross section (RCS) of the target remains constant during the CPI (i.e., the target is coherent). While this assumption

This project is financially supported by the Swedish Foundation for Strategic Research and Sweden's Innovation Agency

does not hold for arbitrarily long CPIs, it is not further addressed in this paper. An arbitrary waveform with a 100 % transmit duty factor is of interest for both digital radar in general and bistatic radar in particular. In related work [23] the single channel bistatic-ambiguity function is introduced, approximated and analyzed. We also note a recent contribution [24], which includes related analyses for a space-air bistatic radar setup and does not transform time into 'fast' and 'slow' dimensions, although it introduces some approximations in time and geometric relations.

A. Notation

Vectors (matrices) are denoted in lower (upper) case bold font. For a real (complex) vector $\boldsymbol{x}$ the transpose (Hermitian transpose) is denoted by $\boldsymbol{x}^T$ ($\boldsymbol{x}^*$). The Euclidean vector norm is $\|\boldsymbol{x}\| = \sqrt{\boldsymbol{x}^*\boldsymbol{x}}$, the Frobenius norm is $\|\boldsymbol{X}\|_{\mathrm{F}} = \sqrt{\mathrm{tr}(\boldsymbol{X}^*\boldsymbol{X})}$ and $\mathrm{vec}\,\boldsymbol{X}$ is the vectorization operator [25].

II. The waveform model

The objective of this section is to give a description of the waveform received at the antenna in the receiving platform (Rx) that is the result of the transmitter (Tx) illumination of a target in space. We assume the target have a constant complex-valued radar cross section. The waveform that arrive at the receiver side of the radar system is hence a scaled and time delayed version of the transmitted waveform. During the CPI we allow the transmitter, receiver and target to move according to their individual constant velocity vectors This implies that the bistatic distance, i.e. the sum of the distance between Tx and target and target and Rx, will vary during the CPI and results in a variation of the wave propagation delay. This propagation delay variation will directly dictate the shape of the received waveform [23]. Without loss of generality we place the origin of the coordinate system at the Tx platform and all positions and velocities will be relative to the Tx platform. We derive the model with the assumption that the relative speed between Tx and Rx platforms is low compared to the EM wave propagation speed and we disregard the Lorentz factor that otherwise would need to be taken into account.

A. The propagation delay

The transmitter antenna emits a waveform that propagate in space. A target, modeled as a point scatterer, with location $\boldsymbol{p}_{\mathrm{S}}(t)$ reflects the waveform and is received by an antenna located at $\boldsymbol{p}_{\mathrm{Rx}}(t)$. With the constant velocity assumption we have the evolvement over time described as

$$\begin{aligned}\boldsymbol{p}_{\mathrm{Rx}}(t) &= \boldsymbol{p}_{\mathrm{Rx},0} + \boldsymbol{v}_{\mathrm{Rx}}t\\ \boldsymbol{p}_{\mathrm{S}}(t) &= \boldsymbol{p}_{\mathrm{S},0} + \boldsymbol{v}_{\mathrm{S}}t\end{aligned} \tag{1}$$

where $\boldsymbol{p}_{\mathrm{Rx},0}$ and $\boldsymbol{p}_{\mathrm{S},0}$ are the receiver and target positions at $t = 0$ and $\boldsymbol{v}_{\mathrm{Rx}}$ and $\boldsymbol{v}_{\mathrm{S}}$ are the velocity vectors respectively. The instantaneous waveform sent out at time t will arrive after a delay of $\tau_{\mathrm{TS}}(t)$ to the target. Hence

$$\tau_{\mathrm{TS}}(t)c = \|\boldsymbol{p}_{\mathrm{S}}(t + \tau_{\mathrm{TS}}(t))\| = \|\boldsymbol{p}_{\mathrm{S},0} + \boldsymbol{v}_{\mathrm{S}}(t + \tau_{\mathrm{TS}}(t))\| \tag{2}$$

where c is the wave propagation speed. Taking squares on both sides in (2) results in

$$\tau_{\mathrm{TS}}^2(t)c^2 = r_{\mathrm{TS}}^2(t) + 2q_{\mathrm{TS}}(t)\tau_{\mathrm{TS}}(t) + \|\boldsymbol{v}_{\mathrm{S}}\|^2\tau_{\mathrm{TS}}^2(t) \tag{3}$$

where

$$r_{\mathrm{TS}}(t) \triangleq \|\boldsymbol{p}_{\mathrm{S}}(t)\| = \|\boldsymbol{p}_{\mathrm{S},0} + \boldsymbol{v}_{\mathrm{S}}t\| \tag{4}$$

is the distance when the waveform leave the transmitter and $q_{\mathrm{TS}}(t)$ is defined as

$$q_{\mathrm{TS}}(t) \triangleq \boldsymbol{p}_{\mathrm{S}}^T(t)\boldsymbol{v}_{\mathrm{S}} = \boldsymbol{p}_{\mathrm{S},0}^T\boldsymbol{v}_{\mathrm{S}} + \|\boldsymbol{v}_{\mathrm{S}}\|^2 t \tag{5}$$

Here $q_{\mathrm{TS}}/r_{\mathrm{TS}}$ is the radial velocity of the target at time t, i.e. the velocity vector of the target projected onto the direction vector from Tx to target. The positive solution to (3) is

$$\tau_{\mathrm{TS}}(t) = \frac{q_{\mathrm{TS}}(t) + \sqrt{q_{\mathrm{TS}}^2(t) + (c^2 - \|\boldsymbol{v}_{\mathrm{S}}\|^2)r_{\mathrm{TS}}^2(t)}}{(c^2 - \|\boldsymbol{v}_{\mathrm{S}}\|^2)} \tag{6}$$

At time $t + \tau_{\mathrm{TS}}(t)$ the target will scatter the instantaneous waveform and the receiving antenna will sense the waveform at time $t+\tau_{\mathrm{TS}}(t)+\tau_{\mathrm{SR}}(t)$ where $\tau_{\mathrm{SR}}(t)$ is the wave propagation time from the target to the receiver (originating from the waveform sent by the transmitter at time t). With the definitions

$$r_{\mathrm{SR}}(t) \triangleq \|\boldsymbol{p}_{\mathrm{Rx},0} - \boldsymbol{p}_{\mathrm{S},0} + (\boldsymbol{v}_{\mathrm{Rx}} - \boldsymbol{v}_{\mathrm{S}})(t + \tau_{\mathrm{TS}}(t))\| \tag{7}$$

as the distance and

$$q_{\mathrm{SR}}(t) \triangleq (\boldsymbol{p}_{\mathrm{Rx},0} - \boldsymbol{p}_{\mathrm{S},0} + (\boldsymbol{v}_{\mathrm{Rx}} - \boldsymbol{v}_{\mathrm{S}})(t + \tau_{\mathrm{TS}}(t)))^T\boldsymbol{v}_{\mathrm{Rx}} \tag{8}$$

the propagation time is given by

$$\tau_{\mathrm{SR}}(t) = \frac{q_{\mathrm{SR}}(t) + \sqrt{q_{\mathrm{SR}}^2(t) + (c^2 - \|\boldsymbol{v}_{\mathrm{Rx}}\|^2)r_{\mathrm{SR}}^2(t)}}{(c^2 - \|\boldsymbol{v}_{\mathrm{Rx}}\|^2)} \tag{9}$$

Consequently, the waveform that was transmitted at time t will be received at time $t + \tau_{\mathrm{TS}}(t) + \tau_{\mathrm{SR}}(t)$ and we define the total delay (propagation time) as

$$\tau(t) = \tau_{\mathrm{TS}}(t) + \tau_{\mathrm{SR}}(t). \tag{10}$$

We note that the mapping from positions and velocities to the delay function $\tau(t)$ is not invertible as there exists several symmetries in the geometry.

B. The received waveform

We assume the transmitter antenna emits an electromagnetic signal $x_{\mathrm{Tx}}(t)$ that is the real part of a complex baseband waveform $s(t)$ modulated by a complex exponential with carrier frequency f_c that is expressed as

$$x_{\mathrm{Tx}}(t) \triangleq \Re(s(t)\exp(j2\pi f_c t)). \tag{11}$$

The waveform transmitted at time t is received at time $t+\tau(t)$. The receiver is assumed to coherently process the signal to baseband by (ideal) mixing and filtering. The complex baseband signal prior to sampling from a specific target associated with the delay $\tau(t)$ is given by

$$x_{\mathrm{Rx}}(t + \tau(t)) \triangleq \alpha s(t)\exp(-j2\pi f_c\tau(t)) \tag{12}$$

where α represents the propagation losses and the complex valued radar cross-section of the target. Consider the time warping function $\zeta(t)$ with domain $t \in (0, \infty)$ and co-domain $t' \in (\tau(0), \infty)$ defined by

$$t' = \zeta(t) \triangleq t + \tau(t) \tag{13}$$

Due to wave propagation properties $\zeta(\cdot)$ is a monotonically increasing function and there exists an inverse $t = \zeta^{-1}(t')$.

With (13), the received baseband signal (12) can be expressed as

$$x_{\text{Rx}}(t') = \alpha s(\zeta^{-1}(t')) \exp(-j2\pi f_c \tau(\zeta^{-1}(t'))) \tag{14}$$

The phase contribution at the receiver due to the carrier is after down mixing given by $-2\pi f_c \tau(\zeta^{-1}(t'))$.

C. Multichannel receiver

The receiver channel model in (14) can be extended to a multichannel receiver with N Rx channels. The received baseband signal at channel number n is then given by

$$x_{\text{Rx},n}(t') = \alpha s(\zeta_n^{-1}(t')) \exp(-j2\pi f_c \tau_n(\zeta_n^{-1}(t'))) \tag{15}$$

where $\zeta_n(t) \triangleq t + \tau_n(t)$ and $\tau_n(t)$ is the channel specific delay function from Tx to Rx antenna channel n (via the target). With a far-field assumption, i.e. the total antenna aperture is much shorter than the distance to the target combined with the natural assumption that all antenna element positions on the Rx platform share the same velocity vector, the expression in (15) can be simplified. Let the relative position of the Rx antenna element n, in relation to the nominal Rx platform position be denoted by $\boldsymbol{p}_{\text{Rx,n}}$. The relative position of the receiver antenna will add a time delay to each received channel compared with the nominal position that depends on the direction of incidence. If we also assume that the bandwidth B of the baseband signal satisfy $\max_n \|\boldsymbol{p}_{\text{Rx,n}}\| < c/B$ then $s(\zeta_n^{-1}(t')) \approx s(\zeta^{-1}(t'))$ and together with the far-field assumption we obtain

$$x_{\text{Rx},n}(t') \approx \alpha a_n(\zeta^{-1}(t')) s(\zeta^{-1}(t')) \exp(-j2\pi f_c \tau(\zeta^{-1}(t'))) \tag{16}$$

where $\zeta(\cdot)$, defined in (13), is the time warping function for the reference position at the Rx platform and the individual delays between the elements results in Rx phase factors given by

$$a_n(t) \triangleq \exp(j\frac{2\pi}{\lambda} \boldsymbol{d}_{\text{RxS}}^T(t) \boldsymbol{p}_{\text{Rx},n}) \tag{17}$$

where $\boldsymbol{d}_{\text{RxS}}(t)$ is the unit norm direction vector pointing from the Rx reference position to the target

$$\boldsymbol{d}_{\text{RxS}}(t) \triangleq \frac{\boldsymbol{p}_{\text{S}}(t + \tau_{\text{TS}}(t)) - \boldsymbol{p}_{\text{Rx},0}(t + \tau(t))}{\|\boldsymbol{p}_{\text{S}}(t + \tau_{\text{TS}}(t)) - \boldsymbol{p}_{\text{Rx},0}(t + \tau(t))\|} \tag{18}$$

and $\lambda = c/f_c$ is the wave length. We note in particular that the direction vector in (18) is time varying to correctly capture the phase variation when the angle to the target is varying during the CPI.

D. The sampled signal

Let T_{CP} denote the processing interval and f_s the baseband sampling frequency and we assume $T_{\text{CP}} f_s$ is integer valued. The signal samples can be arranged into a 2D array of size $T_{CP} f_s \times N$ with elements

$$\boldsymbol{Z}(k, n) \triangleq x_{\text{Rx},n}(k/f_s) \tag{19}$$

where k is the time index and n is the channel number. The vectorization of $\boldsymbol{Z}/\alpha$ can be regarded as the *steering vector* for a given scenario and would be the optimal vector to use in a linear detector if the noise and disturbances would be white.

TABLE I
RADAR PARAMETER VALUES FOR THE 3 SCENARIOS.

Carrier frequency f_c	300 MHz
Pulse rep. int. T_{PR}	0.1 ms
Pulse bandwidth B	10 MHz
Pulse duty cycle η	0.1
Rx sampling freq. f_s	10 MHz
ULA geometry $\boldsymbol{p}_{\text{ULA}}$	$\frac{\lambda}{2}[1, 0, 0]^T$ m

III. EXAMPLE

In this section we explore the use of pulsed waveforms in some bistatic scenarios and see how well the classical model for a multichannel pulse Doppler radar agree with the more correct general waveform model derived in Section II.

A. Pulsed waveforms

Here we introduce the family of pulsed waveforms and the classical approximations that enables fast sequential processing for target detection. A finite waveform $s(t)$ that for $0 \le t < PT_{\text{PR}}$ satisfies

$$\begin{aligned} &s(t) = 0, \quad \eta T_{\text{PR}} \le t < T_{\text{PR}} \\ &s(t + T_{\text{PR}}) = s(t) \end{aligned} \tag{20}$$

is a periodic and pulsed waveform where T_{PR} is the pulse repetition interval, $0 < \eta < 1$ is the pulse duty cycle and P is the number of pulses. In this case $T_{\text{CP}} = T_{\text{PR}} P$.

B. The range-Doppler-angle approximation

When the transmitted waveform is a train of pulses (as in (20) the associated steering vector can be approximated in a way that enables fast and sequential processing. In this section we review the classical range-Doppler-angle approximation of the steering vector where we assume the receiver platform is equipped with a linear uniformly spaced antenna array (ULA) [1]. At the Rx side we sample each antenna channel with sampling frequency f_s and arrange the samples into a 3D array of size $M \times P \times N$, where $M = T_{\text{PR}} f_s$ is the number of samples per period and is assumed to be an integer. The approximation is based on the (incorrect) assumption that the bistatic range, Doppler and angle is the same for all pulses during the CPI. In this work we use the values at time $t' = T_{\text{CP}}/2$ with range

$$r = \|\boldsymbol{p}_{\text{S},0} + \boldsymbol{v}_{\text{S}} t'\| + \|\boldsymbol{p}_{\text{S},0} - \boldsymbol{p}_{\text{Rx},0} + (\boldsymbol{v}_{\text{S}} - \boldsymbol{v}_{\text{Rx}}) t'\| \tag{21}$$

Doppler frequency

$$f_{\text{D}} = \frac{T_{\text{PR}}}{\lambda} (\boldsymbol{v}_{\text{S}}^T \boldsymbol{d}_{\text{TxS}} + (\boldsymbol{v}_{\text{S}} - \boldsymbol{v}_{\text{Rx}})^T \boldsymbol{d}_{\text{RxS}}) \tag{22}$$

and angle frequency

$$f_{\text{a}} = \frac{1}{\lambda} \boldsymbol{p}_{\text{ULA}}^T \boldsymbol{d}_{\text{RxS}} \tag{23}$$

where $\boldsymbol{d}_{\text{TxS}}$ and $\boldsymbol{d}_{\text{RxS}}$ are the unit norm direction vectors that point from Tx to target and Rx to target respectively and $\boldsymbol{p}_{\text{ULA}}^T$ is a vector from the first to second antenna element in the ULA. Based on this mid point in the CPI an approximation of the received data is

$$\boldsymbol{Y}(m, p, n) = s(mf_s - r/c) \exp(j2\pi f_{\text{D}} p + j2\pi f_{\text{a}} n). \tag{24}$$

The vectorization of $\boldsymbol{Y}$ will be an approximate steering vector that also can be described as the Kronecker products between the time shifted pulse (range/fast-time) and two Vandermonde vectors for the Doppler (slow-time) and angle (space) responses respectively. It is clear that this approximation will be less accurate when the CPI increases or if the relative velocities increases. The numerical examples that follow will illustrate this effect.

C. Correlation as performance metric

We evaluate the performance by the magnitude of the correlation between the vectorized matrices defined as

$$C(\operatorname{vec}\boldsymbol{Z}, \operatorname{vec}\boldsymbol{Y}) \triangleq \frac{|\operatorname{vec}(\boldsymbol{Z})^* \operatorname{vec}(\boldsymbol{Y})|}{\|\boldsymbol{Z}\|_{\mathrm{F}}\|\boldsymbol{Y}\|_{\mathrm{F}}}. \tag{25}$$

The quantity C measure the matching between the steering vectors and take values from 0 to 1 where 1 means an ideal match i.e. the vectors $\operatorname{vec}(\boldsymbol{Y})$ and $\operatorname{vec}(\boldsymbol{Z})$ are parallel. The quantity $C(\boldsymbol{a}, \boldsymbol{b})$ is also known as the cosine of the Hermitian angle between the complex vectors $\boldsymbol{a}$ and $\boldsymbol{b}$ [26].

D. Simulation setup

The radar parameters used in the simulation is given in Table I. We simulate three scenarios where the Tx platform is fixed at the origin of the coordinate system and the Rx platform is located at $\boldsymbol{p}_{\mathrm{Rx},0} = [6, 0, 0]^T$ km and stationary. The target initial position is $\boldsymbol{p}_{\mathrm{S},0} = [6, 0.1, 0]^T$ km that is in the broadside direction w.r.t. the ULA in the receiver. The three scenarios are defined as:

S1 $\quad \boldsymbol{v}_{\mathrm{S}} = v[0, 1, 0]^T$ m/s, and $N = 2$.
S2 $\quad \boldsymbol{v}_{\mathrm{S}} = v[1, 0, 0]^T$ m/s, and $N = 2$.
S3 $\quad \boldsymbol{v}_{\mathrm{S}} = v[1, 0, 0]^T$ m/s, and $N = 100$.

In S1 the target moves away from Rx on the radial and the angle stay constant. For S2 and S3 the target moves perpendicular to the radial and the angle variation rate is maximal at $t = 0$. For each scenario, T_{CP} in the set $\{1, 3, 10, 30, 100, 300\}$ ms and velocity v in the set $\{30, 60, 100, 200, 300, 600, 1000, 2000\}$ the correlation C is calculated. Figures 1, 2 and 3 present the results. For all scenarios the correlation decreases with an increasing T_{CP} as well as with an increased target velocity. To obtain a further understanding of what causes the de-correlation we analyse the variations in the bistatic range, the range rate and the angle during the CPI. Let Δr, Δf_{D}, and Δf_{a} denote the difference between the maximum and minimum values of the bistatic range, doppler frequency and angle frequency during the CPI. We normalize these quantities with the classical notion of the resolution respectively in a similar fashion as done in [19]. The normalized quantities are defined as

$$\begin{aligned}
\Delta r_{\mathrm{norm}} &\triangleq \frac{\Delta r}{r_{\mathrm{res}}} = \frac{\Delta r}{c/B} \approx \frac{v T_{\mathrm{CP}} B}{c} \\
\Delta f_{\mathrm{D,norm}} &\triangleq \frac{\Delta f_{\mathrm{D}}}{f_{\mathrm{D,res}}} = \frac{\Delta f_{\mathrm{D}}}{1/P} \approx \frac{2 v T_{\mathrm{CP}}}{\lambda} \\
\Delta f_{\mathrm{a,norm}} &\triangleq \frac{\Delta f_{\mathrm{a}}}{f_{\mathrm{a,res}}} = \frac{\Delta f_{\mathrm{a}}}{1/N} = \frac{\boldsymbol{p}_{\mathrm{ULA}}^T \Delta \boldsymbol{d}_{\mathrm{RxS}} N}{\lambda} = \frac{\boldsymbol{d}_{\mathrm{ULA}}^T \Delta \boldsymbol{d}_{\mathrm{RxS}} N}{2}
\end{aligned} \tag{26}$$

TABLE II
NORMALIZED RANGE, DOPPLER AND ANGLE VARIATION OVER THE CPI AND THE CORRELATION FOR SOME SPECIFIC CASES. IN THE FIGURES A BLACK HEXAGRAM INDICATES THE CASE.

Scenario	S1	S2	S3
v [m/s]	200	100	200
T_{CP} [ms]	100	100	3
Δr_{norm}	**0.68**	0.35	0.02
$\Delta f_{\mathrm{D,norm}}$	0.07	**1.00**	0.003
$\Delta f_{\mathrm{a,norm}}$	0	0.10	**0.30**
Correlation C	0.934	0.954	0.952

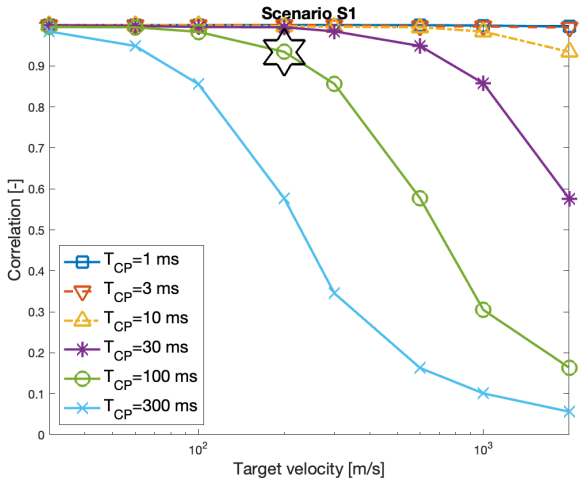

Fig. 1. Correlation as a function of target speed and different CPI. Scenario S1. The hexagram marks the case reported in Table II

where $\Delta \boldsymbol{d}_{\mathrm{RxS}}$ is the variation in the direction vector from Rx to target and $\boldsymbol{d}_{\mathrm{ULA}} \triangleq \frac{2}{\lambda}\boldsymbol{p}_{\mathrm{ULA}}$. For a given T_{CP} and target velocity v we note that Δr_{norm} is proportional to the bandwidth, $\Delta f_{\mathrm{D,norm}}$ is proportional to $1/\lambda$ (or proportional to f_c) and $\Delta f_{\mathrm{a,norm}}$ is proportional to N, the number of antenna channels in Rx. If any of the three relative quantities in (26) approach 1 the correlation between $\boldsymbol{Z}$ and $\boldsymbol{Y}$ starts to decrease. This effect is related to the Kronecker structure of $\operatorname{vec}(\boldsymbol{Y})$. In Table II for each scenario we present the normalized variation for a select velocity and CPI pair. It is clear that S1 is limited by the range variation, S2 by the Doppler variation and S3 by the angle variation. The specific velocity and CPI pair is marked with a black hexagram in the figures.

IV. CONCLUSIONS

A waveform model has been developed that allows arbitrary, non-repetitive waveforms and a 100% transmit duty factor (CW operation). Arbitrary and non-repetitive waveforms are capabilities afforded by a digital radar and CW operation is of large interest for bistatic operations. As such, the model is formulated in time with no split into 'fast' and 'slow' time and thus allows also to analyze performance loss of sub-optimal processing methods. Three bistatic radar examples are analysed using an approximate Kronecker structure (space, fast-time, slow-time) for the received waveform. The described guidelines can be exploited to demonstrate cases where the loss in such Kronecker structure based processing (sequential

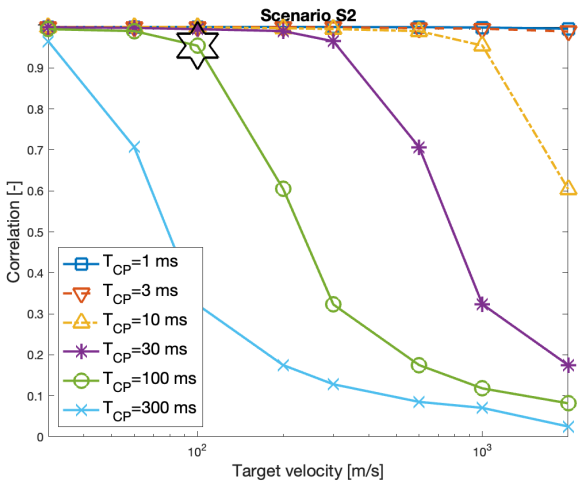

Fig. 2. Correlation as a function of target speed and different CPI. Scenario S2. The hexagram marks the case reported in Table II

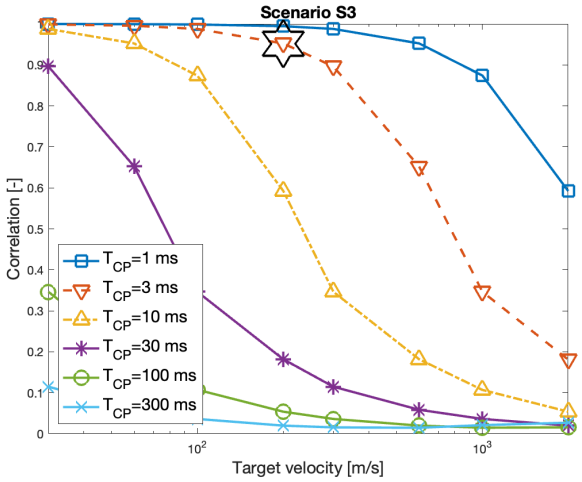

Fig. 3. Correlation as a function of target speed and different CPI. Scenario S3. The hexagram marks the case reported in Table II

processing) becomes non-negligible. Future work will be focused on new ways to find approximate and fast processing schemes for bistatic radar with arbitrary waveforms. The link to the classic ambiguity function and relation to earlier work for Keystone and similar methods and their application in bistatic radar systems will be thoroughly analysed.

REFERENCES

[1] J. R. Guerci, *Space-Time Adaptive Processing for Radar*, 2nd ed. Artech House, 2014.

[2] E. J. Kelly and R. P. Wishner, "Matched-filter theory for high-velocity, accelerating targets," *IEEE Transactions on Military Electronics*, vol. 9, no. 1, pp. 56–69, 1965.

[3] W. J. Caputi, "Stretch: A time-transformation technique," *IEEE Transactions on Aerospace and Electronic Systems*, vol. AES-7, no. 2, pp. 269–278, 1971.

[4] R. K. Raney, "Synthetic aperture imaging radar and moving targets," *IEEE Transactions on Aerospace and Electronic Systems*, vol. AES-7, no. 3, pp. 499–505, 1971.

[5] J. Ender, "Space-time processing for multichannel synthetic aperture radar," *Electronics & Communication Engineering Journal*, vol. 11, no. 1, pp. 29–38, 1999.

[6] J. K. Jao, "Theory of synthetic aperture radar imaging of a moving target," *IEEE Transactions on Geoscience and Remote Sensing*, vol. 39, no. 9, pp. 1984–1992, 2001.

[7] J. Ender, P. Berens, A. Brenner, L. Rossing, and U. Skupin, "Multichannel SAR/MTI system development at FGAN: From AER to PAMIR," in *IEEE International Geoscience and Remote Sensing Symposium*, vol. 3, 2002, pp. 1697–1701 vol.3.

[8] J. H. Ender, "Detection and estimation of moving target signals by multichannel SAR," *Archiv für electronik und ubertragungstechnik*, vol. 50, no. 2, pp. 150–156, 1996.

[9] R. Perry, R. DiPietro, and R. Fante, "SAR imaging of moving targets," *IEEE Transactions on Aerospace and Electronic Systems*, vol. 35, no. 1, pp. 188–200, 1999.

[10] H. Hellsten and L. Ulander, "Airborne array aperture UWB UHF radar-motivation and system considerations," in *Proceedings of the 1999 IEEE Radar Conference. Radar into the next Millennium (Cat. No.99ch36249)*, 1999, pp. 47–53.

[11] M. Pettersson, "Detection of moving targets in wideband SAR," *IEEE Transactions on Aerospace and Electronic Systems*, vol. 40, no. 3, pp. 780–796, 2004.

[12] V. T. Vu, T. K. Sjogren, M. I. Pettersson, A. Gustavsson, and L. M. H. Ulander, "Detection of moving targets by focusing in UWB SAR—theory and experimental results," *IEEE Transactions on Geoscience and Remote Sensing*, vol. 48, no. 10, pp. 3799–3815, 2010.

[13] M. Pettersson, V. Zetterberg, and I. Claesson, "Detection and imaging of moving targets in wide band SAS using fast time backprojection combined with space time processing," in *Proceedings of OCEANS 2005 MTS/IEEE*, 2005, pp. 2388–2393 Vol. 3.

[14] H. Hellsten, "SAR radar system," European Patent EP2 359 159B1, Nov., 2008.

[15] P. Dammert and H. Hellsten, "Focusing ground movers using fast factorized SAR backprojection," in *8th European Conference on Synthetic Aperture Radar*, 2010, pp. 1–4.

[16] R. D. Chapman, C. M. Hawes, and M. E. Nord, "Target motion ambiguities in single-aperture synthetic aperture radar," *IEEE Transactions on Aerospace and Electronic Systems*, vol. 46, no. 1, pp. 459–468, 2010.

[17] K. Kulpa, *Signal Processing in Noise Waveform Radar*. Artech House, 2013.

[18] K. S. Kulpa and J. Misiurewicz, "Stretch processing for long integration time passive covert radar," in *2006 CIE International Conference on Radar*, 2006, pp. 1–4.

[19] F. Pignol, F. Colone, and T. Martelli, "Lagrange-polynomial-interpolation-based keystone transform for a passive radar," *IEEE Transactions on Aerospace and Electronic Systems*, vol. 54, no. 3, pp. 1151–1167, 2018.

[20] O. Jonsson, R. Ragnarsson, T. Sjögren, T. Thor, and A. Tryblom, "An L-band Bistatic Radar: Experimental System and Measurement Campaign," in *Radar 2024*, Rennes, France, Oct. 2024.

[21] K. M. Scott, W. C. Barott, and B. Himed, "The keystone transform: Practical limits and extension to second order corrections," in *2015 IEEE Radar Conference (RadarCon)*, 2015, pp. 1264–1269.

[22] C. Moscardini, D. Petri, A. Capria, M. Conti, M. Martorella, and F. Berizzi, "Batches algorithm for passive radar: A theoretical analysis," *IEEE Transactions on Aerospace and Electronic Systems*, vol. 51, no. 2, pp. 1475–1487, Apr. 2015.

[23] T. Tsao, M. Slamani, P. Varshney, D. Weiner, H. Schwarzlander, and S. Borek, "Ambiguity function for a bistatic radar," *IEEE Transactions on Aerospace and Electronic Systems*, vol. 33, no. 3, pp. 1041–1051, July 1997.

[24] T. Ding, J. Zhang, S. Tang, L. Zhang, and Y. Li, "A novel iterative inner-pulse integration target detection method for bistatic radar," *IEEE Transactions on Geoscience and Remote Sensing*, vol. 60, pp. 1–15, 2022.

[25] A. J. Laub, *Matrix Analysis for Scientists and Engineers*. Siam, 2005, vol. 91.

[26] K. Scharnhorst, "Angles in Complex Vector Spaces," *Acta Applicandae Mathematica*, vol. 69, no. 1, pp. 95–103, Oct. 2001.